Journal of Power Sources 195 (2010) 7152–7159

Contents lists available at ScienceDirect

Journal of Power Sources

journal homepage: www.elsevier.com/locate/jpowsour

Effects of temperature and humidity on the cell performance and resistance of a phosphoric acid doped polybenzimidazole fuel cell

Chen-Yu Chen*, Wei-Hsiang Lai

Institute of Aeronautics and Astronautics, National Cheng Kung University, No. 1, Ta-Hsueh Road, Tainan 701, Taiwan

ARTICLE INFO

Article history:
Received 26 May 2010
Accepted 27 May 2010
Available online 2 June 2010

Keywords:
Proton exchange membrane fuel cell (PEMFC)
Polybenzimidazole (PBI)
Phosphoric acid
Operating temperature
Operating humidity
Electrochemical impedance spectroscopy (EIS)

ABSTRACT

Performance and electrochemical impedance spectroscopy (EIS) tests were performed at different temperatures and humidity levels to understand the effects of temperature and humidity on the performance and resistance of a PBI/H_3PO_4 fuel cell.

The results of the performance tests indicated that increasing the temperature significantly improved the cell performance. In contrast, no improvement was observed when the gas humidity was increased. On the other hand, the EIS results showed that the membrane resistance was reduced for elevated temperatures. This development can be interpreted by the increase in membrane conductivity, as reflected by the Arrhenius equation. As the formation of $H_4P_2O_7$ and the self-dehydration of H_3PO_4 start around 130–140 °C, in PBI, they increase the membrane resistance at temperatures that are higher than 130 °C. In addition, the membrane resistance was reduced for elevated gas humidity levels. This is because an increase in humidity leads to an increase of the membrane hydration level.

The resistance of the catalyst kinetics mainly contributes to the charge transfer resistance. However, under certain conditions, the interfacial charge transfer resistance is also important. It was concluded that the gas diffusion is the main contributor to the mass transfer resistance under dry conditions while it is the gas concentration under humid conditions.

1. Introduction

Fuel cells are among the most promising alternative clean power sources for portable applications and distributed power systems. They may also be viable alternatives in applications for which a highly reliable source of electricity is needed, *e.g.*, in the power systems of automobile and stationary applications.

High temperature membrane (HTM) fuel cells (160–180 °C) are very promising alternative power generation devices because of their high tolerance to carbon monoxide (CO), low dependency on cooling systems, high amount of reusable heat energy, and high practicability in mixed hydrogen systems. They are commonly used in stationary fuel cell systems to enhance the tolerance to reforming gas and reduce the purification cost of a reforming system.

Today, polymer electrolyte membranes for fuel cells can be divided into two broad categories. The first category comprises proton exchange membranes (PEMs) in which only the proton is mobile because the acid anion is covalently linked in the membrane. The second category comprises polymer–acid complexes (PACs) in which both protons and anions are mobile since the acid is simply doped in a basic membrane. For PEM fuel cells, a solvent, *e.g.*, water, is required. For PAC fuel cells, water is not essential [1]. As PAC fuel cells do not highly depend on water, they operate at high temperatures (>100 °C). Several high temperature membrane systems have been reported [2–5]. Among them, a polybenzimidazole-based phosphoric acid-doped (PBI/H_3PO_4) membrane is currently the most successful system because it has high proton conductivity [6], low gas permeability [7], almost zero electro-osmotic drag [1,7,8], good thermal stability [9], and good mechanical properties at temperatures of up to 200 °C. It is well-known that the adsorption of CO on platinum exhibits a high negative function. High operating temperatures reduce the adsorption of CO on platinum. Thus, the catalyst can tolerate a CO concentration of up to 1% [10,11]. The easiest method to enhance the tolerance of a fuel cell to CO is therefore to increase the temperature.

For PBI/H_3PO_4 HTM fuel cells, the optimal operating temperatures range from 150 °C to 200 °C [1,12,13]. However, if the operating temperature is too high, the mechanical stability of the membrane [14] and the operational life of the fuel cell [15,16] are reduced. Furthermore, the fuel cell needs more time to warm up during start-up phases. At high temperatures, the conductivity of the membrane also decreases with operating time [1] because of

* Corresponding author. Tel.: +886 62082848; fax: +886 62389940.
E-mail addresses: p4894101@mail.ncku.edu.tw, aeroshower@msn.com (C.-Y. Chen).

0378-7753/$ – see front matter © 2010 Elsevier B.V. All rights reserved.
doi:10.1016/j.jpowsour.2010.05.057

the evaporation of the doped acid. It is therefore necessary to know the suitable operating temperatures for a PBI/H_3PO_4 HTM fuel cell to obtain a trade-off between the advantages and drawbacks of an operation at a high temperature.

Many researchers have studied the behavior of a PBI/H_3PO_4 HTM fuel cell in dry hydrogen and dry air [17–19]. However, it is almost impossible to supply dry hydrogen and dry air to fuel cells in application systems. In practical situations, the supplied hydrogen often contains water vapor as it is usually supplied from an on-site hydrogen generator (*e.g.*, a reformer) [20–23]. The supplied air also usually contains water vapor because the air pumped into the fuel cell is ambient air [24–26]. It is therefore essential to study the effects of gas humidity on the fuel cell performance to understand the behavior of a PBI/H_3PO_4 fuel cell in a real application system,.

The resistance of a PBI/H_3PO_4 HTM fuel cell is influenced by the relative humidity, temperature, and the acid doping level [1,2,17,27–31]. The ex situ resistance of the membrane at different temperatures, humidity, and acid doping levels and the in situ resistance and performance of the fuel cell at different temperatures and acid doping levels have been reported. Although many researchers have studied the effects of humidity on the ex situ resistance of the membrane, only a few papers have discussed the effects of humidity on the in situ performance and resistance of PBI/H_3PO_4 fuel cells [30]. The effects of humidity on the cell performance and resistance under in situ conditions may be different from that observed under ex situ conditions. Thus, to understand the behavior of a PBI/H_3PO_4 HTM fuel cell, it is essential to study the effects of humidity on the cell performance and electrochemical resistance under in situ conditions.

The objective of this work is to evaluate the performance of PBI/H_3PO_4 HTM fuel cells at different temperatures and gas humidity levels. The electrochemical impedance spectroscopy (EIS) method was utilized for quantifying and discriminating the membrane resistance, charge transfer resistance, and mass transfer resistance.

2. Experimental

2.1. Fuel cell figure

A single cell with a 25 cm^2 active area was used in this study. The flow field geometry was a 5-channel serpentine. The width of the channel, the depth of the channel, and the width of the rib were 0.81 mm, 0.80 mm, and 0.82 mm, respectively. Two heating plates and two T-type thermocouples were attached to the anode and cathode end plates of the fuel cell to control the cell temperature.

2.2. MEA

High temperature PBI membrane electrode assemblies (MEAs) (Celtec®-P Series 1000 [13]), which were provided by the BASF Corporation, were used in this research. The active area of the MEA was 24 cm^2 and the thickness of the MEA was 863 μm. The gaskets were also provided by the BASF Corporation. The thickness of the gasket for the anode was 320 μm and that for the cathode was 345 μm. To ensure a uniform temperature distribution, the single cell was covered by a layer of thermally isolated material. The assembly torques for the 12 bolts were all 7.0 N-m.

2.3. Performance test

A Scribner 850 C test station was used to measure the performance of the fuel cell. Using this test station, voltage, current, and power could be measured and data could be acquired through the data acquisition (DAQ) system. The resolution and accuracy of the current control were 1 mA and 0.3% of the full-scale current rating, respectively. The flow rates of hydrogen and air were controlled by flow controllers via an analog to digital converter. Two bubbling type humidifiers were installed in the test station. The accuracy of the dew point control was ±1 °C. The gas could bypass the humidifier when dry gas was needed for the experiments. The humidity was calibrated before tests. A heating system was used to control the cell temperature. The accuracy of the temperature control was within ±1 °C. In this work, hydrogen with a 99.999% purity was used as the fuel. Air was used as the oxidant instead of pure oxygen because the usage of air is more practical in real applications of fuel cell systems. The basic flow rates of hydrogen and air both were 200 sccm. The stoichiometric ratios of hydrogen (ST_{H_2}) and air (ST_{air}) were 1.2 and 2.0, respectively.

To activate the MEA, the fuel cell was operated at a current density of 0.2 A cm^{-2} for 50 h. After the activation process, the polarization curve at 160 °C was measured. To ensure that the MEA was fully activated, a second polarization curve at 160 °C was measured 24 h after the first polarization curve at 160 °C.

Two MEAs were used in this study. The first one was used for experiments determining the effects of temperature, and the second one was used for experiments determining the effects of humidity. For temperature experiments, only dry hydrogen and dry air were supplied. The sequence of tests was 180 °C, 160 °C, 140 °C, 120 °C, and 70 °C. After the test at 70 °C, a test at 160 °C was again performed. For humidity experiments, hydrogen and air were controlled at the same humidity and the temperature of the fuel cell was kept above 140 °C to avoid water condensation inside the fuel cell. In these tests, the water vapor pressure was used to express the humidity of hydrogen ($P_{H_2O,anode}$) and air ($P_{H_2O,cathode}$). The sequence of tests was dry gas, 0.1 bar, 0.2 bar, 0.3 bar, and 0.4 bar.

Before performing a test under a specific condition, the fuel cell was operated at a current density of 0.25 A cm^{-2} in that specific condition for 1 h to reach the steady state of the system.

2.4. Resistance measurement

In this paper, a Scribner 880 module was used to measure the electrochemical impedance spectroscopy (EIS) of the fuel cell. During measurements, the cell was operated at a stable direct current. A sinusoidal perturbation of the current was added to the DC and a voltage response was obtained. The ratio of the phasor voltage to the phasor current is defined as the impedance of the fuel cell. The AC frequency scanned from 1 kHz to 0.1 Hz. The amplitude of the AC current was 5–10% of the DC current.

Recently, the EIS method has been widely used to study the resistance distribution of fuel cells [32–37] with the aid of equivalent circuit fitting. The intercept on the real axis at high frequency is the sum of the contact resistance ($R_{contact}$), the proton conduction resistance in the membrane ($R_{membrane}$), and the electrical resistance ($R_{electrical}$). The diameter of the arc is the sum of the anodic ($R_{ct,a}$) and cathodic ($R_{ct,c}$) charge transfer resistance and the mass transfer resistance (R_{mt}).

In this work, the current interruption method [38] was also used to measure the membrane resistance of PBI/H_3PO_4 fuel cells and to verify the reliability of the membrane resistance measured by the EIS method. In theory, the cell voltage rises almost instantaneously by the amount of the ohmic potential drop upon the interruption of current. The membrane resistance of the cell, $R_{membrane}$ (ohm cm^2), is determined as the quotient of the instantaneous change in voltage, ΔV (V), and the cell current density, i (A cm^{-2}), just prior to the interruption event. The relation described above is $R_{membrane} = \Delta V/i$.

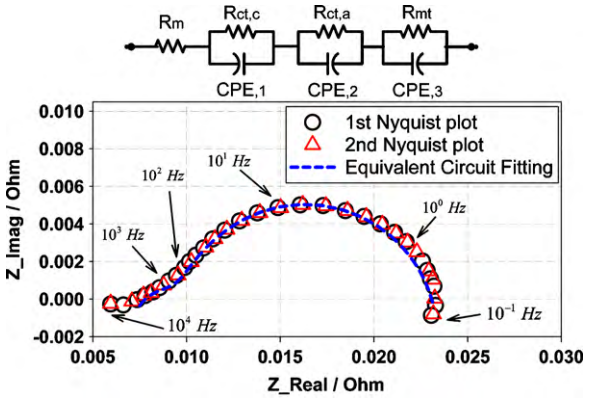

Fig. 1. Nyquist plots at 160 °C and 0.2 A cm^{-2} and the equivalent circuit used in this study (basic flow rate: 200 sccm; ST_{H_2}/ST_{air} : 1.2/2.0; $P_{H_2O,\ anode}/P_{H_2O,cathode}$: 0 bar/0 bar).

3. Results and discussion

3.1. Results of resistance measurement

Fig. 1 shows the results of EIS measurements at 160 °C using dry hydrogen and dry air. The equivalent circuit used in this study is also shown in Fig. 1. To verify the repeatability, two Nyquist plots of EIS tests obtained under the same conditions were compared with each other. It was observed that the two Nyquist plots were almost identical. This result indicates that our EIS measurements had a good repeatability. The equivalent circuit used in this study comprised the contributions of ohmic resistance, anodic charge transfer resistance, cathodic charge transfer resistance, and mass transfer resistance. CPE_1 (constant phase element) represents the $R_{ct,a}$-associated catalyst layer capacitance property. CPE_2 represents the $R_{ct,c}$-associated catalyst layer capacitance property. CPE_3 represents the R_{mt}-associated capacitance property.

As the simulation curve concurs with the experimental results, the equivalent circuit is suitable for the PBI/H_3PO_4 fuel cell used in this study. The ohmic resistance was obtained from the intercept on the real axis. The charge transfer resistance and the mass transfer resistance were obtained by the equivalent circuit fitting. The inductive behavior that was observed at low frequencies (<0.3 Hz) is due to the inductance effect.

3.1.1. Membrane resistance versus current density

In theory, the intercept on the real axis at high frequency (*i.e.*, the ohmic resistance) is the summation of $R_{contact}$, $R_{membrane}$, and $R_{electrical}$. However, $R_{electrical}$ and $R_{contact}$ were previously found to be within the range of 1–10 mohm cm^2 [39–41]. Thus, $R_{electrical}$ and $R_{contact}$ are negligible compared with the proton conduction resistance of the membrane [17,27,28]. The intercept on the real axis at high frequencies can therefore be considered as the membrane resistance, $R_{membrane}$.

Fig. 2 shows the comparison of the membrane resistance measured by the EIS method, R_{EIS}, and the membrane resistance measured by the current interruption method, R_{iR}. The normalized difference $(R_{iR} - R_{EIS})/R_{EIS} \times 100\%$, was found to be between 17.9% and 4.5% at 120 °C and between 15.9% and 3.2% at 160 °C. These results indicate that R_{iR} is greater than R_{EIS}. This is due to the inherent difference in response between the potential distribution within porous electrodes and the non-negligible electrolyte resistance [38]. The normalized differences are in agreement with those reported by Cooper and Smith [38]; these results indicate that the membrane resistance measured in this study is correct.

As can be seen in Fig. 2, the membrane resistance decreases with the increase of the current density at 120 °C and 160 °C. This

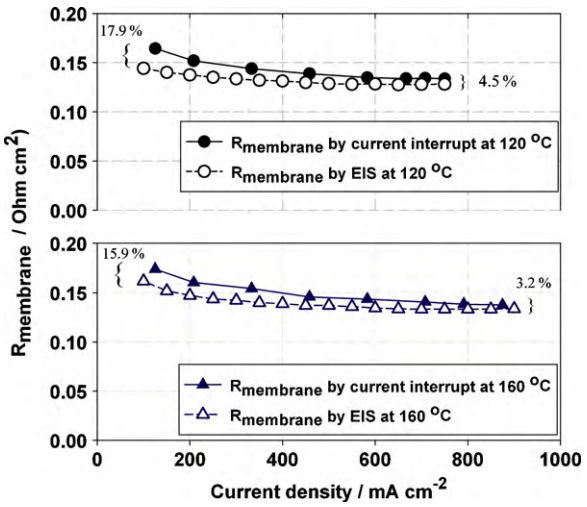

Fig. 2. Comparison between R_{EIS} and R_{iR} at 120 °C and 160 °C (basic flow rate: 200 sccm; ST_{H_2}/ST_{air} : 1.2/2.0; $P_{H_2O,\ anode}/P_{H_2O,cathode}$: 0 bar/0 bar).

observation was previously reported by Zhang et al. [19]. At elevated current densities, the equivalent humidity inside the fuel cell increases due to an increase in the rate of water generation. According to previous ex situ studies on the effects of humidity on the conductivity of PBI/H_3PO_4 membranes [27–29,42], an increase in humidity results in an increase of the number of water molecules adsorbed in the membrane. From a proton transport mechanism perspective, the amount of water adsorbed in the membrane influences the rate of proton conduction. Thus, changing the amount of water adsorbed in the membrane modifies the membrane resistance.

3.1.2. Charge transfer resistance versus current density

Fig. 3 shows the anodic, cathodic, and total charge transfer resistance as functions of the current density. It can be seen that the charge transfer resistance decreases with increasing current densities. In the low current region, the oxygen reduction reaction (ORR) at the cathode dominates while the hydrogen oxidation reaction (HOR) at the anode is negligible. When the current is elevated, the HOR becomes as important as the ORR. The ORR in the low current region, *i.e.*, where the catalyst surface is partially covered by PtO, is controlled by pure electron transfer. However, the ORR in the high current region, *i.e.*, where the catalyst surface is covered by pure

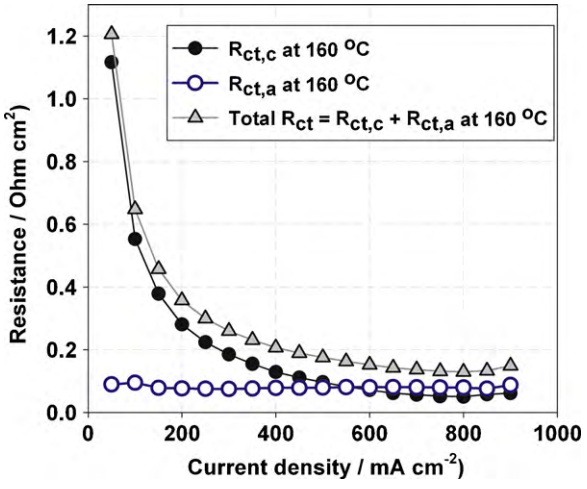

Fig. 3. Change in charge transfer resistance as a function of current density at 160 °C (basic flow rate: 200 sccm; ST_{H_2}/ST_{air} : 1.2/2.0; $P_{H_2O,\ anode}/P_{H_2O,cathode}$: 0 bar/0 bar).

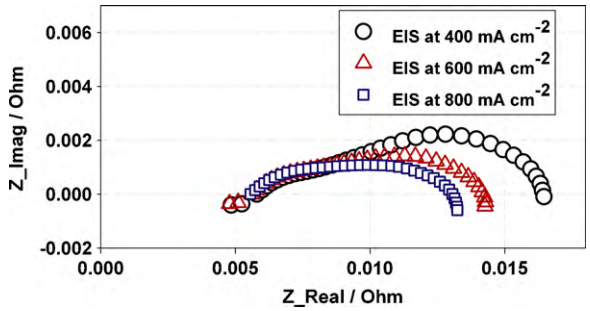

Fig. 4. Nyquist plots at 160 °C for different current densities (basic flow rate: 200 sccm; ST_{H_2}/ST_{air} : 1.2/2.0; $P_{H_2O,\ anode}/P_{H_2O,cathode}$: 0 bar/0 bar).

Pt, is controlled by electron transfer and mass transfer [43]. The HOR occurs on pure Pt for all currents. Thus, $R_{ct,a}$ is much lower than $R_{ct,c}$ in the low current region but is close to $R_{ct,c}$ in the high current region. These results indicate that, a combination of anodic and cathodic charge transfer contributions in the equivalent circuit should be used instead of a cathodic charge transfer contribution when a PBI/H_3PO_4 fuel cell is utilized.

3.1.3. Mass transfer resistance versus current density

If a fuel cell is operated with an insufficient air or hydrogen, the mass transfer resistance contributes the most to the total resistance. For air-breathing fuel cells [44,45], this phenomenon is even more significant. Jalani et al. [30] previously stated that the sum of the charge transfer resistance and the mass transfer resistance did not significantly change when the cathodic flow rate was higher than 0.01 moles min^{-1} at a current density of 0.1 A cm^{-2}, which is equivalent to 224 sccm. It is well-known that the mass transfer resistance is not the main contributor to the impedance when the cathodic basic flow rate or the stoichiometric ratio is high enough [19,46]. Therefore, high basic flow rates of 200 sccm were set for both the anode and the cathode in this study to minimize the influence of the mass transfer resistance. As can be seen in Fig. 4, the mass transfer resistance is not significant for current densities that are lower than 800 mA cm^{-2} because there is no third arc in the low frequency region.

Fig. 5 shows the change of the mass transfer resistance with the current density at 160 °C and 180 °C using dry hydrogen and dry air. As shown in Fig. 5, the mass transfer resistance ranges between 0.02 ohm cm^2 and 0.07 ohm cm^2. It is well-known that the

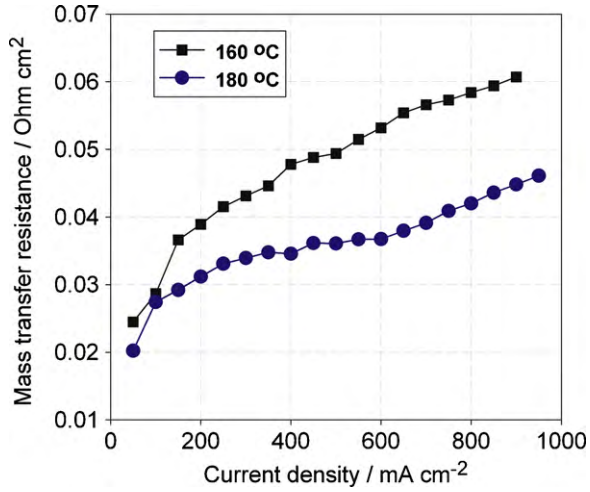

Fig. 5. Change in mass transfer resistance as a function of current density at 160 °C and 180 °C (basic flow rate: 200 sccm; ST_{H_2}/ST_{air} : 1.2/2.0; $P_{H_2O,\ anode}/P_{H_2O,cathode}$: 0 bar/0 bar).

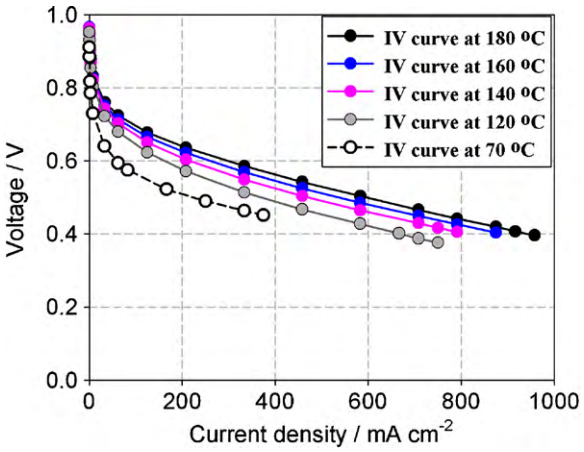

Fig. 6. Effects of the temperature on the IV curves (basic flow rate: 200 sccm; ST_{H_2}/ST_{air} : 1.2/2.0; $P_{H_2O,\ anode}/P_{H_2O,cathode}$: 0 bar/0 bar).

main contributor to the cell resistance at high current densities is the mass transfer resistance because the gas concentration in the gas diffusion layer decreases at elevated current densities [47,48]. However, the mass transfer resistance measured in this paper is much lower than the membrane resistance and the charge transfer resistance in the low current region. It is also slightly lower than the membrane resistance and the charge transfer resistance in the high current region. These results indicate that a proper gas supply strategy can minimize the influence of the mass transfer resistance.

3.2. Temperature effects on fuel cell performance

Fig. 6 shows the effects of temperature on IV curves using dry hydrogen and dry air. As can be seen, the performance increases with the increase of temperature. The voltages at 333 mA cm^{-2} at 180 °C, 160 °C, 140 °C, 120 °C, and 70 °C are 0.586 V, 0.569 V, 0.549 V, 0.514 V, and 0.464 V, respectively. As shown in Fig. 6, the temperature has a significant effect on the performance of the cell at temperatures lower than 140 °C. However, there is no significant effect at temperatures higher than 140 °C.

3.3. Effects of temperature on fuel cell resistance

Fig. 7 shows the change of membrane resistance with the reciprocal of temperature for different current densities. Previous ex situ studies showed that the conductivity of the membrane increased

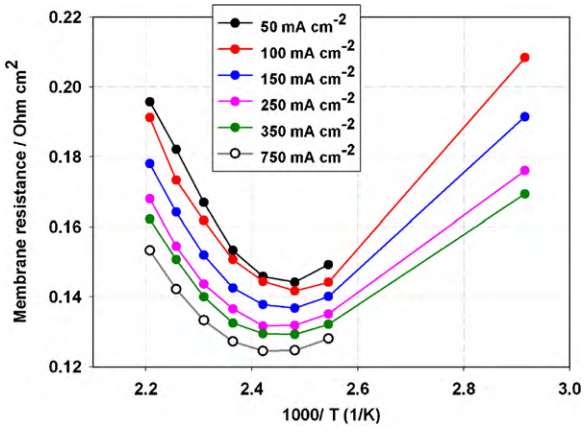

Fig. 7. Change in membrane resistance as a function of the reciprocal of the temperature for different current densities (basic flow rate: 200 sccm; ST_{H_2}/ST_{air} : 1.2/2.0; $P_{H_2O,\ anode}/P_{H_2O,cathode}$: 0 bar/0 bar).

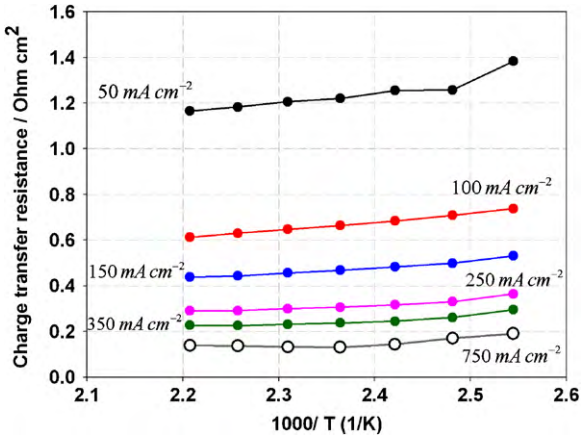

Fig. 8. Change in the total charge transfer resistance as a function of the reciprocal of the temperature for different current densities (basic flow rate: 200 sccm; ST_{H_2}/ST_{air} : 1.2/2.0; $P_{H_2O,\ anode}/P_{H_2O,cathode}$: 0 bar/0 bar).

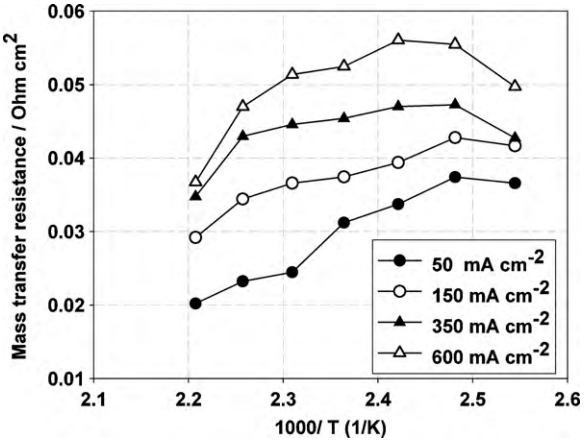

Fig. 9. Change in mass transfer resistance as a function of the reciprocal of the temperature for different current densities (basic flow rate: 200 sccm; ST_{H_2}/ST_{air} : 1.2/2.0; $P_{H_2O,\ anode}/P_{H_2O,cathode}$: 0 bar/0 bar).

with the increase of temperature according to the Arrhenius equation [6,17,27]. Previous in situ studies on PBI/H_3PO_4 fuel cells also showed that the cell performance increased with the increase of temperature [19,30,31]. In our study, the increase of the temperature led to a better cell performance between 70 °C and 180 °C. However, the membrane resistance did not increase when the temperature was increased in this temperature range.

Ma et al. [28] previously reported that the formation of $H_4P_2O_7$ (Eq. (1)) under dry conditions starts at around 130–140 °C in PBI. Thus, the proton transfer paths above and below 130 °C might be different under dry conditions. Lobato et al. [31] found that increasing the temperature (to temperatures higher than 140 °C) reduced the level of hydration of the membrane and accelerated the self-dehydration of H_3PO_4. Both groups concluded that the loss of water in the membrane and the formation of $H_4P_2O_7$ might decrease the proton conductivity. Thus, the increase in the membrane resistance above 130 °C observed in this study can be attributed to the dehydration of the membrane and the formation of pyrophosphoric acid.

In addition, the lowest membrane resistance was observed at 130 °C for low current densities (<150 mA cm^{-2}) and at 140 °C for high current densities (>150 mA cm^{-2}). The shift in the lowest point of resistance is due to the change in current density, which results in a change of the hydration level of the PBI membrane.

$$2H_3PO_4 \rightarrow H_4P_2O_7 + H_2O \quad (1)$$

Fig. 8 represents the change of total charge transfer resistance with the reciprocal of the temperature for different current densities. The charge transfer resistance decreases with an increase of the temperature. According to the Bulter–Volmer equation, increasing the temperature leads to an increase in the reaction rate constant and results in a considerable enhancement of the fuel cell reaction kinetics. Zhang et al. [19] and Oono et al. [17] both reported such observation.

As can be seen in Fig. 8, the discrepancy in the resistance at low and high temperatures decreases with the increase of the current density, which is due to the fact that the charge transfer resistance is coupled with the mass transfer resistance. In the low current region, the ORR is only controlled by electron transfer. On the other hand, in the high current region, it is controlled by both electron transfer and mass transfer. When temperature is increased in the high current region, the mass transfer resistance increases due to a decrease in the gas concentration in the diffusion layer [19]. Therefore, the negative contribution of the increase of the mass transfer resistance partly offsets the positive contribution of the increase of the electron transfer rate at elevated temperatures.

Fig. 9 shows the change of the mass transfer resistance with the reciprocal of the temperature for different current densities. The mass transfer is mainly controlled by the rate of gas diffusion and the gas concentration in the diffusion medium (or gas solubility) [47,49]. While increasing the temperature leads to an increase in the rate of gas diffusion, it leads to a decrease of the gas concentration in the diffusion layer. At elevated temperatures, the mass transfer is a combination of the negative contribution that results from the decrease in the gas concentration and the positive contribution that results from the increase of the gas diffusion rate.

As can be seen in Fig. 9, the mass transfer resistance decreases with increasing temperatures above 140 °C, while it increases with increasing temperatures below 130 °C. The location of the peak resistance seems to shift from 130 °C to 140 °C when the current density increases from 50 mA cm^{-2} to 600 mA cm^{-2}. From a mass transfer mechanism perspective, the gas diffusion rate may be the main contributor under dry conditions (high temperatures and low currents) and the gas concentration may be the main contributor under humid conditions (low temperatures and high currents). Oono et al. [17] have concluded that the mass transfer resistance decreased with increasing temperatures between 150 °C and 190 °C at 0.2 A cm^{-2} because the gas diffusion rate was the main contributor. Zhang et al. [19] have stated that the gas concentration was the main contributor between 160 °C and 200 °C for current densities that are greater than 1.0 A cm^{-2}. The results of these two previous studies support our conclusions.

3.4. Fuel cell performance and resistance before and after the test at 70 °C

In experiments on the effects of temperature, the test sequence was 180 °C, 160 °C, 140 °C, 120 °C, 70 °C, and 160 °C. Fig. 10 shows the comparison of the cell performances at 160 °C before and after the test at 70 °C. The duration of the test at 70 °C was 1.5 h. The performance dropped significantly after the test at 70 °C. Indeed, the voltage at 333 mA cm^{-2} was 0.569 V before the test at 70 °C while it was 0.537 V after the test. As can be seen in Fig. 11, the charge transfer resistance did not change after the test at 70 °C. However, the membrane resistance increased significantly after the test at 70 °C. The PBI/H_3PO_4 membrane resistance is mainly influenced by the temperature, humidity, and acid doping levels. In this experiment, the temperature and humidity in the two tests were identical. Therefore, the increase of the membrane resistance may be attributed to the decrease in acid doping levels [2,18], *i.e.*, to the loss of acid when the cell was operated at 70 °C. Acid loss may

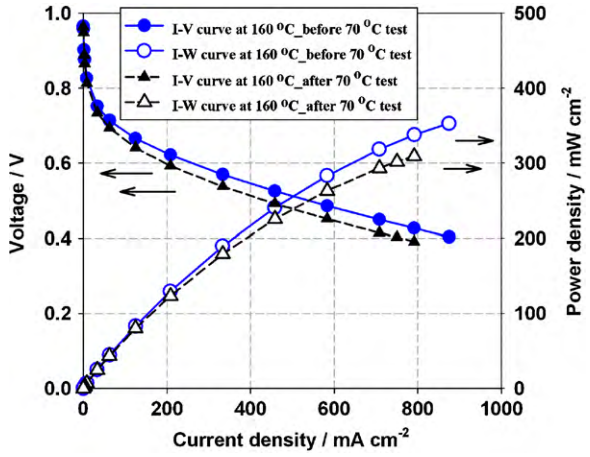

Fig. 10. Cell performance at 160 °C before and after the test at 70 °C *t* (duration of the test at 70 °C: 1.5 h; basic flow rate: 200 sccm; ST_{H_2}/ST_{air} : 1.2/2.0; $P_{H_2O,\ anode}/P_{H_2O,cathode}$: 0 bar/0 bar).

occur via different mechanisms, such as diffusion, capillary transport, membrane compression, evaporation, and leaching caused by condensed water during shutdowns and cold starts. In our case, we believe that the acid leached out due to liquid water. Thus, further efforts are required to prevent acid loss when the fuel cell is operated at dynamic temperatures.

3.5. Effects of humidity on fuel cell performance

Fig. 12 shows the change of the cell performance with the water vapor pressure at 160 °C for different current densities. As can be seen, the effects of humidity on a PBI fuel cell is less significant than the effects of humidity on a Nafion membrane fuel cell. This is due to the fact that the conductivity of a PBI membrane is less dependent on water than that of a Nafion membrane. The minimum number of water molecules adsorbed per sulphonic site needs to be between 6 and 7 for a Nafion membrane [50]. On the other hand, the number of water molecules adsorbed per PBI repeat unit is only of about 3 [27], and the number of water molecules adsorbed per H_3PO_4 molecule is between 0 and 1.1 [51,52]. Thus, it can be concluded that the effects of humidity on the performance of a PBI fuel cell is not significant.

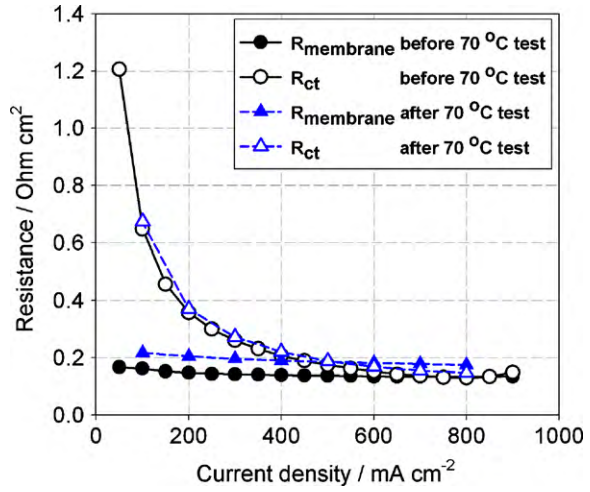

Fig. 11. Cell resistance at 160 °C before and after the test at 70 °C (basic flow rate: 200 sccm; ST_{H_2}/ST_{air} : 1.2/2.0; $P_{H_2O,\ anode}/P_{H_2O,cathode}$: 0 bar/0 bar).

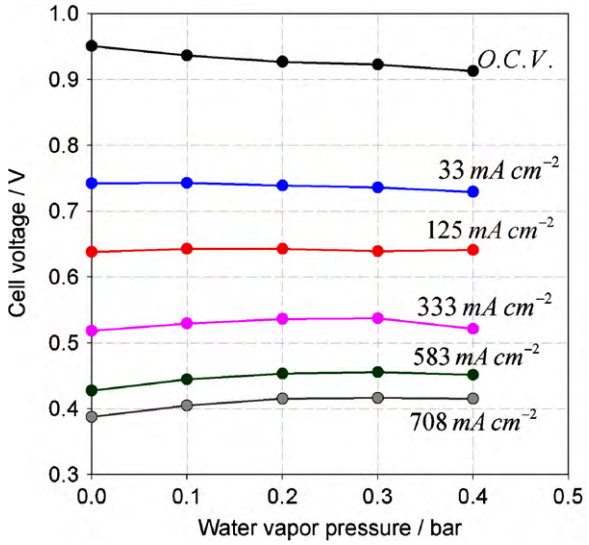

Fig. 12. Change in cell performance as a function of the water vapor pressure at 160 °C for different current densities (basic flow rate: 200 sccm; ST_{H_2}/ST_{air} : 1.2/2.0).

As shown in Fig. 12, the open circuit voltage (OCV) decreases with the increase of the water vapor pressure. This can be interpreted using the Nernst equation (Eq. (2)). From a thermodynamic point of view, an increase of the water vapor pressure results in a reduction of the OCV.

$$E^{OCV} = E^0 + \frac{RT}{2F} \ln\left(\frac{P_{H_2} P_{O_2}^{1/2}}{P_{H_2O}}\right) \quad (2)$$

For current densities between 33 mA cm^{-2} and 333 mA cm^{-2}, the cell voltage did not change significantly when the water vapor pressure was changed. On the other hand, for current densities greater than 583 mA cm^{-2}, the cell voltage slightly increased when the water vapor pressure was increased. These results indicate that the difference between the OCV and the voltage for a specific current density decreases when the humidity is increased. This is due to the fact that an increase in humidity results in a decrease of the membrane resistance, which in its turn results in a decrease of the voltage difference according to the Ohm's law, $\Delta V = iR_{membrane}$.

The decrease of the membrane resistance for high humidity levels is discussed below.

3.6. Effects of humidity on fuel cell resistance

Fig. 13 shows the change of the membrane resistance with the water vapor pressure at 160 °C for different current densities. The membrane resistance decreased with the increase of the gas humidity. Wippermann et al. [53] observed a similar phenomenon. In their work, the membrane resistance was reduced when the fuel was switched from dry hydrogen to humidified hydrogen. This phenomenon may be attributed to the increase of the amount of water that is adsorbed in the membrane.

As reported in the literature, the water content in the fuel cell membrane affects the proton conductivity and the fuel cell performance. Thus, the effects of humidity on the membrane conductivity for Nafion membranes [54,55] and PBI membranes [6,27,28,42,56] have been thoroughly studied to understand the proton conduction mechanism.

Pu et al. [57] proposed that the proton transport in a PBI/H_3PO_4 membrane involves two mechanisms, the Grotthuss mechanism [58] and the vehicle mechanism [59]. The Grotthuss mechanism states that protons are transported by a rapid proton exchange via hydrogen bonds between solvent molecules, which include acid

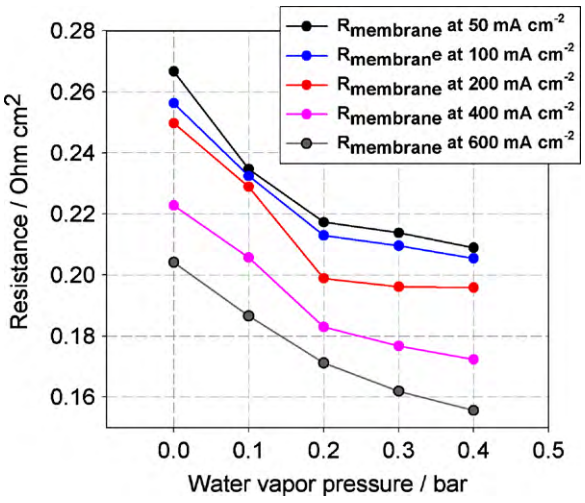

Fig. 13. Change in membrane resistance as a function of the water vapor pressure at 160 °C for different current densities (basic flow rate: 200 sccm; ST_{H_2}/ST_{air} : 1.2/2.0).

molecules, the heterocyclic PBI nitrogens, and the water molecules. The vehicle mechanism states that protons are transported by self-diffusion of acid and water molecules.

In the two proton transport mechanisms, increasing the number of water molecules in the membrane can increase the proton conductivity by either increasing the proton diffusion rate or the probability of proton hopping via hydrogen bonds as water molecules can act as an additional protic solvent (Eq. (3)) in the PBI/H_3PO_4 system, which also increases the proton transport rate.

$$H_3PO_4 + H_2O \rightarrow H_2PO_4^- + H_3O^+ \quad (3)$$

Fig. 14 shows the change of the total charge transfer resistance with the water vapor pressure at 160 °C for different current densities. At 50 mA cm^{-2}, the charge transfer resistance decreased with the increase of the water vapor pressure. At 100 mA cm^{-2} and 200 mA cm^{-2}, the charge transfer resistance did not change significantly when the humidity was modified. For current densities greater than 400 mA cm^{-2}, it increased slightly with the increase of the water vapor pressure. The charge transfer resistance contributes to the resistance of the catalyst kinetics, the interfacial charge transfer resistance on the electrolyte side ($R_{ct,E}$) [60], and the interfacial charge transfer resistance on the reactant side ($R_{ct,R}$) [43]. The resistance of the catalyst kinetics is independent of the gas humidity over the entire current range, but $R_{ct,E}$ and $R_{ct,R}$ are influenced by both the current density and the gas humidity.

In the low current region, the reactant adsorbed on the catalyst surface was saturated and $R_{ct,R}$ was almost constant. However, $R_{ct,E}$ varied because the water content between the electrolyte and the catalyst was not saturated. Therefore, increasing the humidity resulted in an increase of the water content at the interface between the electrolyte and the catalyst (*i.e.*, it increased the Pt surface area covered by the electrolyte) and in a decrease of $R_{ct,E}$ [60]. On the other hand, in the high current region, the rate of water generation was high and the water content between the electrolyte and the catalyst was almost saturated. Consequently, $R_{ct,E}$ was considered to be constant in the high current region. On the other hand, $R_{ct,R}$ became variable because the reactant on the catalyst surface was not saturated. Therefore, in the high current region, the increase in humidity (*i.e.*, the decrease of the reactant concentration in the diffusion layer) increases the charge transfer resistance by increasing $R_{ct,R}$ [43]. Although it was observed that the charge resistance changed when the humidity was modified, the effects of humidity at 160 °C are minor. This is due to the fact that the PBI/H_3PO_4 high temperature membrane fuel cell is not really water dependent.

Fig. 15 shows the change of the mass transfer resistance with the water vapor pressure at 160 °C for different current densities. The mass transfer resistance increased with increasing humidity. In Section 3.3, we concluded that the gas concentration mainly contributed to the mass transfer resistance under humid conditions. Thus, the increase of the mass transfer resistance in Fig. 15 is due to the decrease of the reactant concentration that results from the increased humidity. Nakamura et al. [61] have found that the mass transfer resistance significantly increased when the humidity was increased for a Nafion-based PEMFC at 80 °C. The reason for the decrease of the mass transfer resistance was that liquid water partially covered the catalyst layer and blocked the flow channels. In this study, the fuel cell was operated above 100 °C and the water molecules inside the fuel cell were therefore gaseous. Thus, the mass transfer resistance of the high temperature membrane fuel cell was not subject to the change of the effective catalyst area and the flooding phenomenon in flow channels when the humidity was changed. These are the reasons why the changes in the mass transfer resistance are minor (<0.035 ohm cm^2), as seen in Fig. 15.

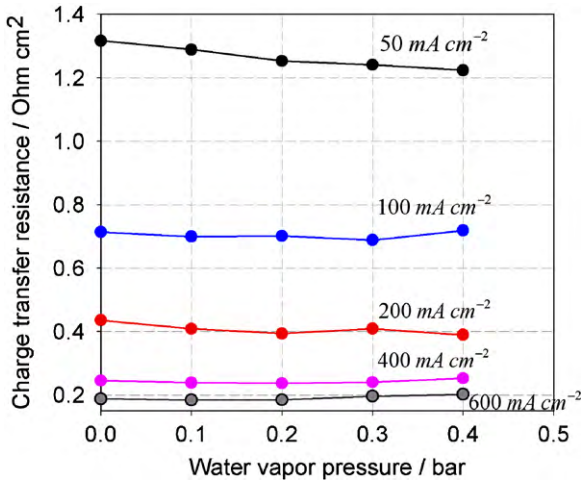

Fig. 14. Change in total charge transfer resistance as a function of the water vapor pressure at 160 °C for different current densities (basic flow rate: 200 sccm; ST_{H_2}/ST_{air} : 1.2/2.0).

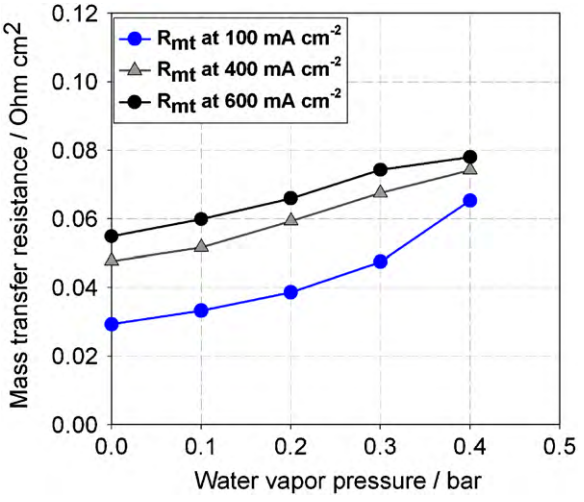

Fig. 15. Change in mass transfer resistance as a function of the water vapor pressure at 160 °C for different current densities (basic flow rate: 200 sccm; ST_{H_2}/ST_{air} : 1.2/2.0).

4. Conclusions

Based on the EIS analysis of the PBI/H_3PO_4 fuel cell, it is recommended to use a combination of anodic and cathodic charge transfer contributions in the equivalent circuit instead of a cathodic charge transfer contribution because the HOR becomes as important as the ORR for elevated current densities.

The experimental results on the effects of the temperature and humidity indicate that the cell performance is significantly improved by increasing the temperature but not by increasing the gas humidity. The membrane resistance was reduced at elevated temperatures because the membrane conductivity was increased according to the Arrhenius equation. It was also reduced for elevated gas humidity levels because of the hydration of the membrane. In addition, increasing the temperature simultaneously reduces the hydration level of the membrane. The formation of $H_4P_2O_7$ and the self-dehydration of H_3PO_4 also starts at around 130–140 °C in PBI. Thus, increasing the temperature decreases the membrane resistance at temperatures that are lower than 130 °C and increases the membrane resistance at temperatures that are higher than 140 °C.

The charge transfer resistance decreases with increasing temperatures and decreases with increasing gas humidity levels in the low current region. However, it slightly increases with increasing gas humidity levels in the high current region. Although the charge transfer resistance is mainly affected by the resistance of the catalyst kinetics, our results show that the interfacial charge transfer resistance on the electrolyte side and the interfacial charge transfer resistance on the reactant side are considerable under certain conditions.

In conclusion, the gas diffusion rate is the main contributor to the mass transfer resistance under dry conditions while it is the gas concentration under humid conditions.

The PBI/H_3PO_4 fuel cell should not be operated below 100 °C because the cell performance can be reduced due to the acid loss that results from the leaching caused by condensed water.

Acknowledgments

This project was supported by the National Science Council (NSC), Taiwan, under the contract no. NSC 97-2622-E-006-028-CC2. The authors thank the Taiwan National Science Council and the Celxpert Energy Corporation for their financial support.

References

[1] Q. Li, J.O. Jensen, R.F. Savinell, N.J. Bjerrum, Progress in Polymer Science 34 (2009) 449–477.
[2] B. Xing, O. Savadogo, Journal of New Materials for Electrochemical Systems 2 (1999) 95–101.
[3] W.H.J. Hogarth, J.C.D.d. Costa, G.Q.M. Lu, Journal of Power Sources 142 (2005) 223–237.
[4] S. Vengatesan, H.-J. Kim, S.-Y. Lee, E. Cho, H. Ha, I.-H. Oh, S.-A. Hong, T.-H. Lim, International Journal of Hydrogen Energy 33 (2008) 171–178.
[5] Y.M. Kim, S.H. Choi, H.C. Lee, M.Z. Honga, K. Kima, H.-I. Leeb, Electrochimica Acta 49 (2004) 4787–4796.
[6] J.S. Wainright, J.-T. Wang, D. Weng, R.F. Savinell, M. Litt, Journal of Electrochemical Society 142 (1995) L121–L123.
[7] D. Weng, J.S. Wainright, U. Landau, R.F. Savinell, Journal of Electrochemical Society 143 (1996) 1260–1263.
[8] X. Ren, W. Henderson, S. Gottesfeld, Journal of Electrochemical Society 144 (1997) L267–L270.
[9] S.R. Samms, S. Wasmus, R.F. Savinell, Journal of Electrochemical Society 143 (1996) 1225–1232.
[10] J.D. Holladay, J.S. Wainright, E.O. Jones, S.R. Gano, Journal of Power Sources 130 (2004) 111–118.
[11] Q. Li, R. He, J.-A. Gao, J.O. Jensen, N.J. Bjerrum, Journal of Electrochemical Society 150 (2003) A1599–A1605.
[12] J. Lebæk, S.T. Ali, P. Møller, C. Mathiasen, L.P. Nielsen, S.K. Kær, International Journal of Hydrogen Energy (2009), doi:10.1016/j.ijhydene.2009.10.002.
[13] T.J. Schmidt, J. Baurmeister, Journal of Power Sources 176 (2008) 428–434.
[14] R. He, Q. Li, A. Bach, J.O. Jensen, N.J. Bjerrum, Journal of Membrane Science 277 (2006) 38–45.
[15] J. Xie, D.L.W.D.M. Wayne III, T.A. Zawodzinski, P. Atanassov, R.L. Borupa, Journal of Electrochemical Society 152 (2005) A104–A113.
[16] K. Yasuda, A. Taniguchi, T. Akita, T. Ioroi, Z. Siroma, Physical Chemistry Chemical Physics 8 (2006) 746–752.
[17] Y. Oono, T. Fukuda, A. Sounai, M. Hori, Journal of Power Sources 195 (2010) 1007–1014.
[18] Y. Oono, A. Sounai, M. Hori, Journal of Power Sources 189 (2009) 943–949.
[19] J. Zhang, Y. Tang, C. Song, J. Zhang, Journal of Power Sources 172 (2007) 163–171.
[20] A.T. Ashcroft, A.K. Cheetham, M.L.H. Green, P.D.F. Vernon, Nature 352 (1991) 225–226.
[21] R.-F. Horng, H.-H. Huang, M.-P. Lai, C.-S. Wen, W.-C. Chiu, International Journal of Hydrogen Energy 33 (2008) 3719–3727.
[22] R.-F. Horng, M.-P. Lai, H.-H. Huang, Y.-P. Chang, Energy Conversion and Management 50 (2009) 2632–2637.
[23] E.C. Vagia, A.A. Lemonidou, International Journal of Hydrogen Energy 32 (2007) 212–223.
[24] H.-P. Chang, C.-L. Chou, Y.-S. Chen, T.-I. Hou, B.-J. Weng, International Journal of Hydrogen Energy 32 (2007) 316–322.
[25] J.J. Hwang, D.Y. Wang, N.C. Shih, Journal of Power Sources 141 (2005) 108–115.
[26] J.-H. Wee, Renewable and Sustainable Energy Reviews 11 (2007) 1720–1738.
[27] R. He, Q. Li, G. Xiao, N.J. Bjerrum, Journal of Membrane Science 226 (2003) 169–184.
[28] Y.-L. Ma, J.S. Wainright, M.H. Litt, R.F. Savinell, Journal of Electrochemical Society 151 (2004) A8–A16.
[29] Q. Li, R. He, R.W. Berg, H.A. Hjuler, N.J. Bjerrum, Solid State Ionics 168 (2004) 177–185.
[30] N.H. Jalani, M. Ramani, K. Ohlsson, S. Buelte, G. Pacifico, R. Pollard, R. Staudt, R. Datta, Journal of Power Sources 160 (2006) 1096–1103.
[31] J. Lobato, P. Cãnizares, M.A. Rodrigo, J.e.J. Linares, Electrochimica Acta 52 (2007) 3910–3920.
[32] J.-P. Diard, N. Glandut, P. Landaud, B.L. Gorrec, C. Montella, Electrochimica Acta 48 (2003) 555–562.
[33] N. Fouquet, C. Doulet, C. Nouillant, G. Dauphin-Tanguy, B. Ould-Bouamama, Journal of Power Sources 159 (2006) 905–913.
[34] A. Hakenjos, M. Zobel, J. Clausnitzer, C. Hebling, Journal of Power Sources 154 (2006) 360–363.
[35] T. Romero-Castañón, L.G. Arriaga, U. Cano-Castillo, Journal of Power Sources 118 (2003) 179–182.
[36] R.-H. Song, D.-J. Kim, C.-S. Kim, D.-R. Shin, Journal of New Materials for Electrochemical Systems 4 (2001) 47–50.
[37] X. Yuan, H. Wang, J.C. Sun, J. Zhang, International Journal of Hydrogen Energy 32 (2007) 4365–4380.
[38] K.R. Cooper, M. Smith, Journal of Power Sources 160 (2006) 1088–1095.
[39] L. Zhang, Y. Liu, H. Song, S. Wang, Y. Zhou, S.J. Hu, Journal of Power Sources 162 (2006) 1165–1171.
[40] Zhiliang Wu, Y. Zhou, G. Lin, Shuxin Wang, S.J. Hu, Journal of Power Sources 182 (2008) 265–269.
[41] P. Zhou, C.W. Wu, G.J. Ma, Journal of Power Sources 159 (2006) 1115–1122.
[42] M.K. Daletou, J.K. Kallitsis, G. Voyiatzis, S.G. Neophytides, Journal of Membrane Science 326 (2009) 76–83.
[43] C. Song, Y. Tang, J.L. Zhang, J. Zhang, H. Wang, J. Shen, S. McDermid, J. Li, P. Kozak, Electrochimica Acta 52 (2007) 2552–2561.
[44] C.-Y. Chen, W.-H. Lai, B.-J. Weng, H.-J. Chuang, C.-Y. Hsieh, C.-C. Kung, Journal of Power Sources 179 (2008) 147–154.
[45] J.J. Hwang, C.H. Chao, Electrochimica Acta 52 (2007) 1942–1950.
[46] W.-M. Yan, C.-Y. Chena, S.-C. Meia, C.-Y. Soong, F. Chen, Journal of Power Sources 162 (2006) 1157–1164.
[47] S. Shimpalee, U. Beuscher, J.W.V. Zee, Journal of Power Sources 163 (2006) 480–489.
[48] F.-B. Weng, A. Su, G.-B. Jung, Y.-C. Chiu, S.-H. Chan, Journal of Power Sources 145 (2005) 546–554.
[49] S. Shimpalee, D. Spuckler, J.W.V. Zee, Journal of Power Sources 167 (2007) 130–138.
[50] T.E. Springer, T.A. Zawodzinski, S. Gottesfeld, Journal of Electrochemical Society 138 (1991) 2334–2342.
[51] L.A. Diaz, G.C. Abuin, H.R. Corti, Journal of Power Sources 188 (2009) 45–50.
[52] J. Lobato, P. Cañizares, M.A. Rodrigo, J.J. Linares, G. Manjavacas, Journal of Membrane Science 280 (2006) 351–362.
[53] K. Wippermann, C. Wannek, H.-F. Oetjen, J. Mergel, W. Lehnert, Journal of Power Sources 195 (2010) 2806–2809.
[54] D.J. Burnett, A.R. Garcia, F. Thielmann, Journal of Power Sources 160 (2006) 426–430.
[55] T.J.P. Freire, E.R. Gonzalez, Journal of Electroanalytical Chemistry 503 (2001) 57–68.
[56] O.E. Kongstein, T. Berning, B. Børresen, F. Seland, R. Tunold, Energy 32 (2007) 418–422.
[57] H. Pu, W.H. Meyer, G. Wegner, Journal of Polymer Science Part B: Polymer Physics 40 (2002) 663–669.
[58] R. Bouchet, E. Siebert, Solid State Ionics 118 (1999) 287–299.
[59] K.D. Kreuer, Journal of Membrane Science 185 (2001) 29–39.
[60] F. Liu, B. Yi, D. Xing, J. Yu, Z. Hou, Y. Fu, Journal of Power Sources 124 (2003) 81–89.
[61] S. Nakamura, H. Nishikawa, T. Aoki, Y. Ogami, Journal of Power Sources 186 (2009) 278–285.